Title: Experimental and numerical study on the regeneration performance of LiCl solution with surfactant and nanoparticles

Author: Tao Wen, Lin Lu * (vivien.lu@polyu.edu.hk), Hong Zhong, Chuanshuai Dong

Department of Building Services Engineering, The Hong Kong Polytechnic University, Hong Kong, China

Abstract: The paper experimentally and numerically investigated the enhancement of LiCl falling film regeneration performance in a plate type regenerator by adding surfactant polyvinyl pyrrolidone (PVP) and multi-walled carbon nanotubes (MWNTs). Experimentally, by adding surfactant PVP and adopting mechanical methods, steady nanofluid containing MWNTs was successfully fabricated. The regeneration characteristics of LiCl/H_2O solution, LiCl/H_2O-PVP solution and LiCl/H_2O-MWNTs nanofluid were identified quantitatively. Compared with the regeneration rate of the LiCl/H_2O solution, the values of the LiCl/H_2O-PVP solution and nanofluid are on average 24.9% and 24.7% greater. These enhancements can be attributed to the increase of mass transfer area and decrease of falling film thickness, which is caused by a decrease in contact angles. However, adding 0.1 wt% MWNTs to the LiCl/H_2O-PVP solution has negligible influence on the regeneration rate. The three solutions have nearly the same mass transfer coefficients under comparable operating conditions. Theoretically, a mathematical model was built with the consideration of film contraction to describe the simultaneous heat and mass transfer processes in the regenerator. The calculated falling film wetting areas agree well with the measured ones, with a relative difference of less than 6%. The mean absolute relative deviation between the computational regeneration rates and experimental ones for the LiCl/H_2O solution, LiCl/H_2O-PVP solution and LiCl/H_2O-MWNTs nanofluid are 9.01%, 3.95% and 4.22%, respectively, which demonstrates the accuracy of the developed model. The experimental data and newly developed numerical model are helpful for the study of regeneration enhancement and system design of liquid desiccant cooling systems.

Key words: surfactant, nanofluid, mass transfer enhancement, falling film regenerator,

mathematical model

Nomenclature			
c_p	Heat capacity ($kJ/(kg.K)$)	β	Shrinkage angle (^{o})
D	Rim part length (m)	δ	Film thickness (m)
g	Gravitational acceleration (m^2/s)	γ	Vapourisation latent heat (kJ/kg)
h	Enthalpy (kJ/kg)	μ	Dynamic viscosity ($Pa.s$)
L	Dehumidifier Length (m)	θ	Contact angle (^{o})
Le	Lewis number	ρ	Density (kg/m^3)
$LDCS$	Liquid desiccant cooling system	σ	Surface tension (N/m)
m	Mass flow rate (kg/s)	ξ	Deformation factor
MWNT	Multi-walled carbon nanotube	Δ	Change value
p	Pressure (Pa)	Subscripts	
Pr	Prandtl number	a	Air
PVP	Polyvinyl pyrrolidone	cal	Calculated result
Re	Reynolds number	exp	Experimental results
Sc	Schmidt number	e	Equilibrium
Sh	Sherwood number	h	Heat transfer
w	Absolute humidity (g/kg)	i	Inlet
T	Temperature (^oC)	m	Mass transfer/main part
X	Concentration ($\%$)	o	Outlet
Greek symbols		r	Rim part
α_h	Heat transfer coefficient ($W/(m^2K)$)	s	Solution
α_m	Mass transfer coefficient ($kg/(m^2.s)$)	w	Cooling water

1 Introduction

The regenerator is one of the main components in a liquid desiccant cooling system (LDCS), which is promising technology for air-conditioning due to its energy saving potential and accurate temperature and humidity control [1]. During the process of regeneration, low-grade energy, such as solar energy and waste water heat [2], can be utilised. Given the high proportion of energy (30% to 50%) consumed by air-conditioning systems [3], the attractions of LDCS are clear. To further enhance heat and mass transfer performance during the regeneration or dehumidification process, various physical and chemical methods have been proposed by researchers.

Surface modification is the most direct way to enhance mass transfer during regeneration. Some novel configurations, such as constant curvature surface (CCS) [4], surface treatment tubes [5, 6], film-inverting structures [7, 8] and plate-fin

structures [9], have been studied by previous investigators. Most of these surface modification methods attempt to change the flow pattern on the absorber or regenerator to increase turbulent flow and ensure a greater contact area for heat and mass transfer. Aside from configuration enhancement, surface treatment with super-hydrophilic coating is also an effective way to improve the surface wettability of the regenerator or dehumidifier [10].

Other methods focus on modification of the liquid desiccant itself rather than the configuration of components in the LDCS, such as adding surfactant or nanoparticles to the solution. For the surfactant, a minor amount of certain chemical substances, such as 2-ethyl-1-hecanol [11], 2-methyl-1-pentanol [12] and n-octanol [13], was mixed into the desiccant solution. Different degrees of mass transfer enhancement were experimentally observed in previous studies [11-13]. Most researchers attributed the enhancement mechanism to Marangini convection. However, the attribution of the trigger mechanism for Marangini convection is still controversial. Some possible explanations, such as the Kashiwagi model [14], salting-out model [15], solubility model [16] and vapour surfactant theory [17], have been proposed. However, only a partial enhancement phenomenon could be explained this way, rather than all surfactants.

Nanofluid is defined as a steady lyosol containing nanoparticles with a size of less than 100 nm [18]. Methods for the preparation of nanofluid can be divided into two groups: one-step and two-step. The former fabricates and disperses nanoparticles simultaneously into a base fluid [19]. Generally speaking, this method performs better than the two-step method. Nevertheless, the complicated manufacturing processes involved and low production output restrict its large-scale application. In the two-step method, nanoparticles are produced by physical and chemical synthesis techniques [19]. Subsequently, the prepared nanoparticles are dispersed into a base fluid by various methods. This method has been widely used in both research and commercial applications due to its low cost. Because of its outstanding thermal physical properties, nanofluid has become a hot research area in recent years.

Numerous studies have concentrated on heat transfer enhancement by adding nanoparticles into water or other base fluids. Both single phase and multiphase heat transfer experiments and numerical studies were carried out to uncover the heat transfer characteristics in nanofluid. Different levels of improvement in terms of the heat transfer coefficient were revealed [20]. Compared with the large amount of research concerning heat transfer, investigations focusing on mass transfer are relatively scarce. Mass transfer studies of nanofluid have concentrated on gas absorption and liquid mass diffusion [21, 22]. The types of gas absorption mainly include bubble type and falling film. Falling film water vapour dehumidification, which is the research focus of this study, belongs to the latter type.

Kang et al. [23] studied the absorption performance of $LiCl/H_2O$ solution with the addition of Fe and carbon nanotubes in a tube type absorber. They adopted Arabic gum as a surfactant and used an ultrasonic vibrator to obtain stable nanofluid dispersion. The experimental results showed that the mass transfer enhancement of carbon nanotubes was greater than that of Fe, by a factor of up to 2.48 at a concentration of 0.1 wt%. Kim et al. [24] performed a similar study with the addition of SiO_2 nanoparticles. They found that the nanoparticles could be steadily dispersed into the $LiBr/H_2O$ solution only when the concentration of SiO_2 was less than 0.01 vol%. Otherwise, distribution stabilisation was required. Mass transfer improvement could be increased up to 18% at the SiO_2 concentration of 0.005 vol%, which was caused by Brownian motion, as stated by Kim et al. [24]. Fe_3O_4 was adopted by Zhang et al. [25] to study the falling film absorption experimentally. Their results indicated that the absorption enhancement ratio increased with the increase of the mass fraction of Fe_3O_4 and a decrease in particle size. The enhancement ratio reached up to 2.28 at a concentration of 0.05 wt% for 20 nm nanoparticles. The working pair of $LiBr/H_2O$ was replaced by NH_3/H_2O in the study conducted by Yang et al. [26]. Three kinds of nanoparticles, Al_2O_3, Fe_2O_3 and $ZnFe_2O_4$, were added into the base fluid of NH_3/H_2O solution. They found that the absorption rate was weakened by adding poorly dispersed nanoparticles or only adding surfactant. The absorption

performance of Fe_2O_3 could be increased by 70% with the matched surfactant under certain circumstances. Pineda et al. [27] studied CO_2 absorption performance in a tray column absorber using methanol with the addition of Al_2O_3 and SiO_2 nanoparticles. During the preparation of nanofluids, an ultra-sonicator was used for the dispersion of nanoparticles. Pineda et al.'s results indicated that the maximum enhancement ratios for Al_2O_3 and SiO_2 were 9.4% and 9.7%, respectively. In addition to experimental studies, some researchers have conducted numerical studies. Ali et al. [28, 29] numerically investigated dehumidification performance in vertical and inclined plate falling film absorbers with the addition of Cu-ultrafine particles.

However, apart from Ali et al. [28, 29], all of the preceding studies of gas absorption focus on absorption refrigeration operated in a closed loop; for example, the operation pressures of Kang et al. [23] and Kim et al. [24] were both 0.01 bar. However, mass and heat transfer in the LDCS occur in an open loop at atmospheric pressure. Furthermore, no study has paid attention to the regeneration process, which is an indispensable part in the LDCS, and Ali et al. [28, 29] did not take the dispersion of nanoparticles into consideration, which is a practical and serious problem in nanofluid research.

In this study, a stable 0.1 wt% $LiCl/H_2O$-MWNTs nanofluid was first fabricated by adding surfactant PVP and adopting mechanical methods. Then, with a purpose-built test bench, comparative experiments were conducted with $LiCl/H_2O$ solution, $LiCl/H_2O$-PVP solution and nanofluid to identify regeneration performance under various operating conditions. Finally, a mathematical model that takes film shrinkage on the regenerator into consideration was developed and validated.

2 Experimental method

2.1 Nanofluid fabrication and stability analysis

The MWNTs used in this study were purchased from Suzhou Hengqiu Graphene Co. Ltd. Some characteristic parameters are given in Table 1. To obtain a stable nanofluid, the surfactant PVP was used along with mechanical stirring and ultrasonic vibration. The detailed dispersion processes are shown in Fig. 1. It is worth noting

that a stable nanofluid can be obtained by regulating the pH value of the solution [30]. The LiCl solution used in this study had a pH value of around 5.2, which was measured by a pH tester with an accuracy of 0.1. Some researchers have controlled the pH using hydrochloric acid and sodium hydroxide [30]. However, in this study, adopting such a solution modifier may have a negative effect on the mass transfer performance of the LiCl solution. Therefore, we used a tiny amount of surfactant for the steady dispersion of nanofluid. Dispersion solutions with PVP concentrations of 0 wt%, 0.1 wt%, 0.2 wt%, 0.3 wt% and 0.4% wt were prepared individually for comparison at a MWNTs concentration of 0.1 wt %. The stabilities of the five solutions after 60 days of sediment are presented in Fig. 2 [31]. It can be observed that the solution without the adding of PVP subsided totally, and when the PVP concentration was less than 0.4 wt%, different levels of sediment were revealed. As a result, this study uses a PVP concentration of 0.4 wt% for the subsequent regeneration study. The particle distribution of nanofluid was also obtained using a Mastersizer 3000 laser diffraction particle size analyser made by Malvern Company. The outcomes are shown in Fig. 3. As can be seen, there are two centralised sections for particle size distribution, which is caused by the non-circular structure of MWNTs and corresponds to the diameter and length of nanotubes. As the particle distribution curves at 0 and 60 days indicate, obvious aggregation of particles does not occur. Consequently, the MWNTs are steadily dispersed into the LiCl/H_2O solution in a manner appropriate for the following experiments.

Table 1. Some characteristics of MWNTs.

Parameter	Inner diameter (nm)	Outer diameter (nm)	Length (um)	Density (g/cm^3)	Production method
Specification	3-5	8-15	3-12	1.8	CVD*

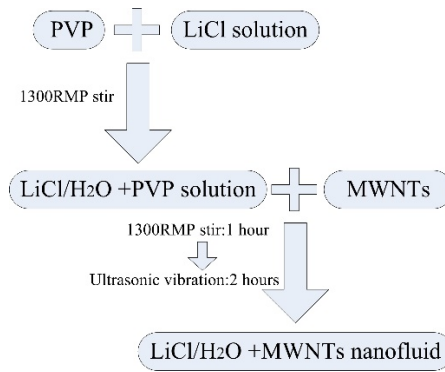CVD*: Chemical Vapour Deposition

Fig. 1. Dispersion processes of LiCl/H_2O-MWNTs nanofluid.
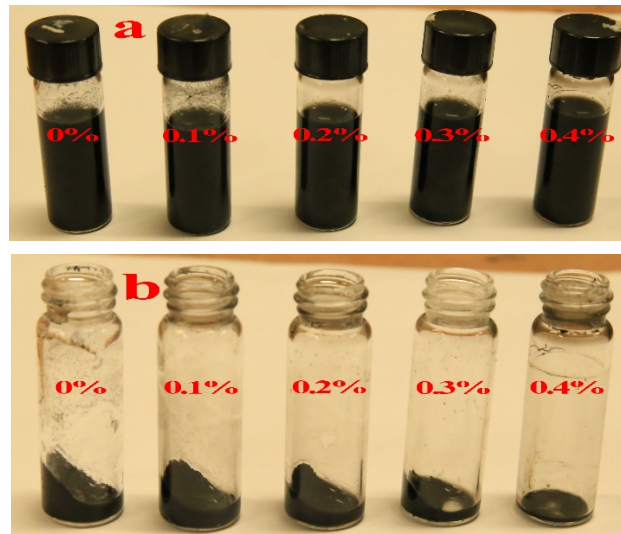

Fig. 2. Dispersion results under different PVP concentrations: (a) 0 days, (b) 60 days.
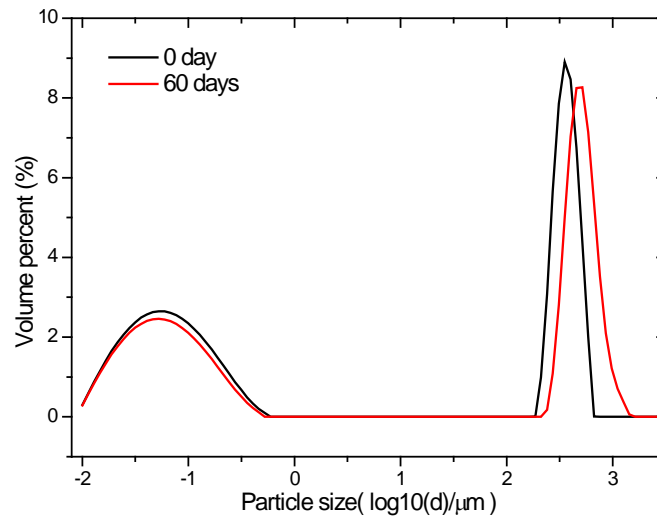

Fig. 3. Particle distribution of the LiCl/H_2O-MWNTs nanofluid.

2.2 Experimental system description

A test bench, as shown in Fig. 4, was built to investigate the regeneration performance of the three kinds of solution [32]. The whole system has three loops: the

solution loop, air loop and hot water loop. All of the loops were insulated from the ambient environment by neoprene foam. For the solution loop, the weak solution was installed in a tank connected to a pump. After being heated to the desired temperature by an electrical heater, the weak solution was pumped into the loop. The flow rate of the solution was controlled by regulating the opening angle of a three-way valve. The flow rate was measured by a turbine flow rate meter with an accuracy of 3%. A distributor was used to uniformly distribute the solution on the plate regenerator. The plate regenerator was made of 316L stainless steel with the size of 500 mm * 500 mm (width*length). After the simultaneous heat and mass transfer in the single channel plate regenerator, the solution was collected by a container connected to another solution tank. Both the inlet and outlet solution temperatures were measured by Pt-100 thermocouples with an accuracy of 0.1 K. The solution concentration was obtained indirectly according to the equation provided by Conde [33]. The density was first obtained using a specific gravity hydrometer with an accuracy of 1 kg/m^3. Then, combined with the solution temperature, the concentration could be obtained by the relevant correlation from Conde [33].

Air from the ambient environment was sucked into the air duct by a fan. To study the influence of air temperature and inlet humidity on regeneration characteristics, a heater and a humidifier were installed in the duct. The air flow rate could also be regulated by a damper, and was measured by a Pitot tube with an uncertainty of 2.5%. Two humidity sensors installed at the duct's inlet and outlet were used to measure the dry bulb temperatures and relative humidity with an accuracy of 0.1 K for temperature and 2.5% for relative humidity. Internal heating was adopted to improve regeneration performance. Hot water was provided by a heating tank and pumped into the regenerator by a pump. The flow patterns of the hot water/solution and solution/air were both counter-flow. After heat exchange with the solution, the water flowed back to the heating tank for the next cycle. The inlet and outlet water temperatures were obtained by two Pt-100 thermocouples. Another turbine flow rate meter was used to measure the water's flow rate.

solution flow rate, solution temperature, air flow rate, air dry bulb temperature and air humidity. The specifications of the operating conditions are summarised in Table 2.
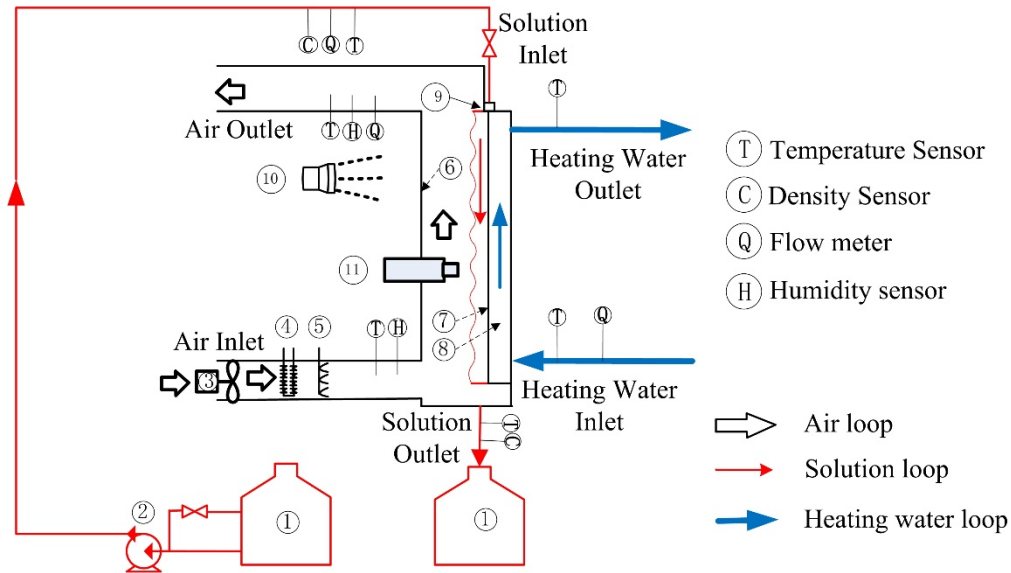
1、Solution tanks   2、Solution pump   3、Air fan   4、Air heater   5、Regenerator
6、Air channel 7、Working surface 8、Internally heating unit 9、Solution distributor
10、Infrared thermal imager   11. Accumeasure instrument

Fig. 4. Schematic diagram of the test bench.

Table 2. Specification of the experimental working conditions

Material	Parameter	Range
Solution	Concentration (wt%)	34
	Mass flow rate (kg/s)	0.07~0.16
	Inlet temperature (^{o}C)	48, 50, 52, 55
Regeneration air	Inlet humidity (g/kg)	13~25
	Mass flow rate (kg/s)	0.023~0.065
	Dry bulb temperature (^{o}C)	27.5~36
Heating water	Mass flow rate (kg/s)	0.12
	Inlet temperature (^{o}C)	51, 53, 55, 58
PVP	Concentration (wt%)	0.4
MWNTs	Concentration (wt%)	0.1

2.3 Regeneration performance index

The purpose of regeneration is to evaporate water from the weak solution and make it stronger. Therefore, the most direct way to evaluate regeneration performance is the concentration difference between the inlet and outlet solutions. However, experiments revealed that the difference in concentration over one cycle is too tiny to

be measured accurately. As a result, in the present study we chose an indirect way to evaluate regeneration performance, called the regeneration rate. Its definition is given in Equation (1):

$$\Delta m = G_a.(d_{a,o} - d_{a,i})$$ (1)

where the mass flow rate of air is presented by G_a and d is the absolute humidity, which is obtained by Equation (2). The subscripts a, o, i for d stand for air, inlet and outlet, respectively. The formulation represents the total air moisture change, which is equal to the amount of water evaporated from the solution.

$$d = f(T_{dry}, \varphi)$$ (2)

where T_{dry} represents the air dry-bulb temperature and φ is the relative humidity.

The mass transfer coefficient is also used to evaluate the regeneration performance, as defined by Equation (3):

$$h_m = \frac{G_a}{A} \frac{d_{a,o} - d_{a,i}}{d_e - d_{a,i}}$$ (3)

where A is the wetting area of the falling film and d_e is the equivalent humidity content of liquid desiccant in the condition of equilibrium at its concentration and temperature.

2.4 Uncertainty analysis and experimental validation

Parameters such as temperature, flow rate, relative humidity and density were measured directly by sensors. Therefore, their uncertainties depend on the accuracy of the sensors. Indirectly obtained parameters such as concentration, absolute humidity and regeneration rate are calculated by certain correlations. Their uncertainties are obtained by the uncertainty propagation method [34], which is formulated in Equation (4).

$$\delta Y = \sqrt{(\frac{\partial Y}{\partial x_1} \delta x_1)^2 + (\frac{\partial Y}{\partial x_2} \delta x_2)^2 + ... + (\frac{\partial Y}{\partial x_n} \delta x_n)^2}$$ (4)

where the uncertainty of Y is given by δY. All of the uncertainties involved in this study are summarised in Table 3.

Table 3. The uncertainties of different parameters.

Parameter	Uncertainty	Parameter	Uncertainty
Temperature/T	$\pm 0.1K$	Solution density/ ρ_s	$\pm 1kg/m^3$
Air relative humidity/ φ	$\pm 2.5\%$	Solution concentration/ X_s	0.2%
Solution flow rate/ G_s	$\pm 3\%$	Air absolute humidity/ d	2.8%
Cooling water flow rate/ G_w	$\pm 3\%$	Regeneration rate/ Δm	4.9%
Air flow rate/ G_a	$\pm 2.2\%$	Mass transfer coefficient / h_m	5.1%

As simultaneous heat and mass transfer occur during the regeneration process, conservation laws in terms of heat balance and mass balance must be satisfied. Their expressions are specified in Equations (5) and (6). However, concerning the mass conservation of Equation (5), as stated earlier, the concentration change between inlet and outlet solutions was too small to be measured. Consequently, only the heat conservation equation in Equation (6) is checked, and the validation results are illustrated in Fig. 5. Almost all of the absolute differences of enthalpies are less than 25%. As a result, the rationality of the experimental system is demonstrated.

$$G_s(h_{s,o} - h_{s,i}) = G_w(h_{w,i} - h_{w,o}) + G_a(h_{a,i} - h_{a,o}) \tag{5}$$

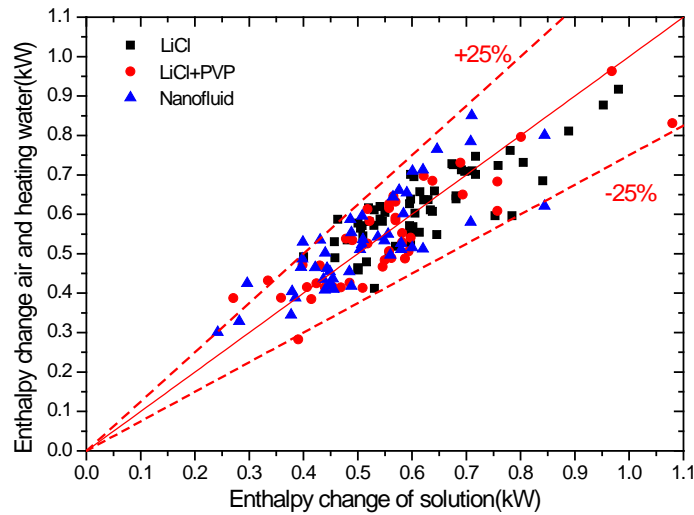$$G_a(d_{a,i} - d_{a,o}) = G_s X_{s,i}(\frac{1}{X_{s,o}} - \frac{1}{X_{s,i}}) \tag{6}$$

Fig. 5. Validation results of the energy balance.

3. Regeneration performance and discussion

3.1 Influence of solution temperature

The effect of solution temperature on regeneration performance is set out in Fig. 6. One can see that the regeneration rate increases with the increase of solution temperature for all three solutions, which is caused by an increase in mass transfer driving force. When the solution temperature changes from 48°C to 55°C at the concentration of 34%, the equivalent water vapour content at the solution surface increases from 24.2 g/kg to 35.5 g/kg correspondingly. However, the mass transfer coefficient decreases as the solution temperature increases. The regeneration rates for the LiCl/H$_2$O-PVP solution and nanofluid both show an obvious enhancement compared with the LiCl/H$_2$O solution, as indicated in Fig. 6. However, no clear difference can be detected between the LiCl/H$_2$O-PVP solution and nanofluid in terms of the regeneration rate. For the mass transfer coefficient, all three solutions share comparable values under the same operating conditions.
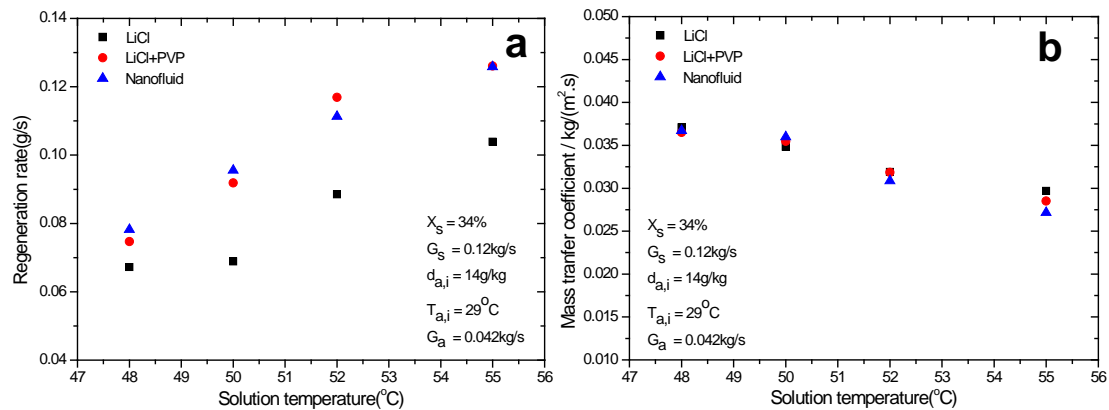

Fig. 6. Influence of solution temperature on regeneration performance.

3.2 Influence of solution flow rate

Fig. 7 gives the effect of solution flow rate on regeneration characteristics. Both the regeneration rates and mass transfer coefficient fluctuate around certain values, even though the mass flow rate nearly doubles, from 0.075 kg/s to 0.16 kg/s. The regeneration rate are 0.0617 g/s, 0.0745 g/s and 0.0780 g/s, respectively, for the given solutions. This relatively small change can be mainly attributed to the minor impact of solution flow rate on mass transfer coefficient, as shown in Fig. 7-b. Mass transfer coefficient remains at around 0.0267 kg/(m^2.s) for different solution flow rates under the experimental conditions given in Fig. 7. An absolute regeneration rate increase of 0.0129 g/s and 0.0163 g/s is obtained for the LiCl/H$_2$O-PVP solution and nanofluid.

For the two modified solutions, the regeneration rates are more or less the same.

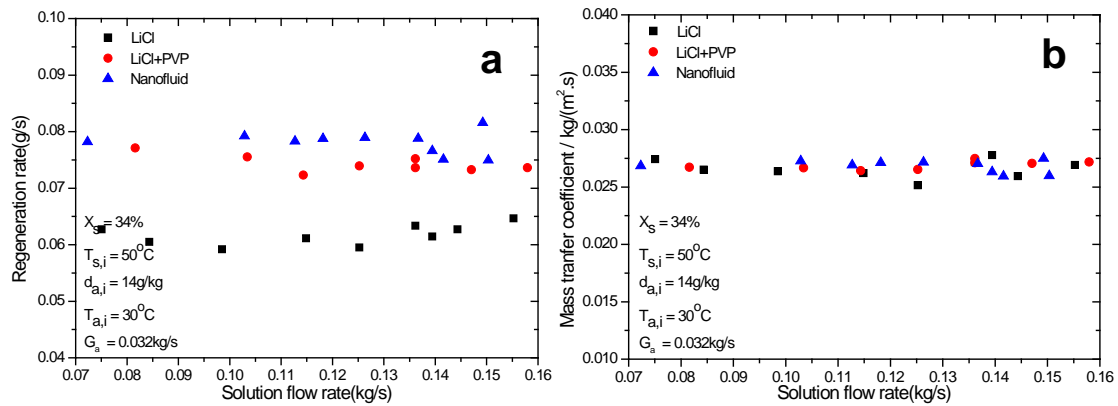

Fig. 7. Influence of solution flow rate on regeneration performance.

3.3 Influence of air temperature

Fig. 8 shows the regeneration rates and mass transfer coefficients under different air temperatures ranging from 27.5°C to 36°C. Even though the temperature increases by approximately 9°C, the regeneration rates remain at stable values, namely 0.0841 g/s, 0.1051 g/s and 0.1049 g/s, for the LiCl/H_2O solution, LiCl/H_2O-PVP solution and nanofluid. The mass transfer coefficient fluctuates around 0.0225 kg/(m^2.s) for the three liquid desiccants. Relative enhancements of 25.0% and 24.7% in terms of regeneration rate are shown for the two modified solutions. The effect of MWNTs on regeneration rate can not be detected by comparing the experimental results between the LiCl/H_2O-PVP solution and nanofluid, as shown in Fig. 8.
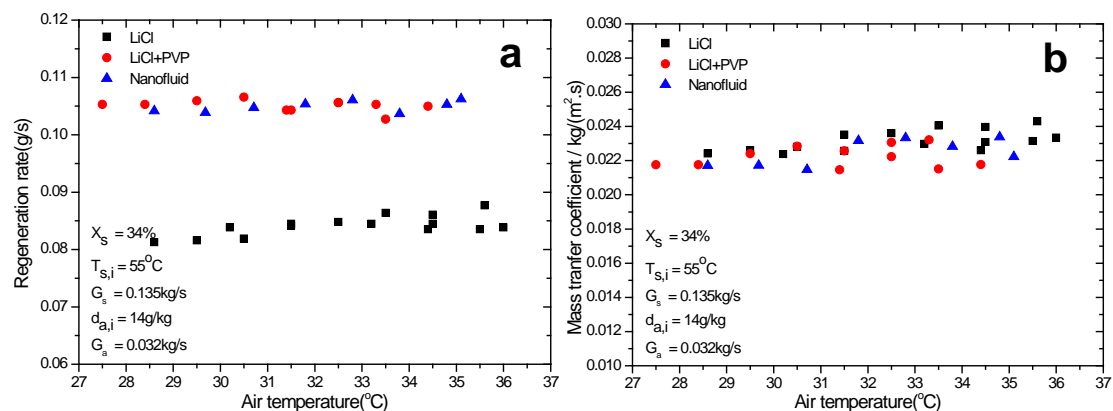

Fig. 8. Influence of air temperature on regeneration performance.

3.4 Influence of air flow rate

Fig. 9 shows the influence of air flow rate on regeneration performance. It is clear that as air flow rate increases, both the regeneration rate and mass transfer

coefficient increase for all three solutions. This trend in the regeneration rate results from the increase of mass transfer coefficient, as shown in Fig. 9-b. For instance, the mass transfer coefficient for the LiCl/H$_2$O solution increases from 0.0219 kg/(m^2.s) to 0.0464 kg/(m^2.s) when the air flow rate changes from 0.023 kg/s to 0.066 kg/s. Similar to the previous results, the two modified solutions show a distinct improvement in regeneration rate. The LiCl/H$_2$O-PVP solution and nanofluid also share comparable enhancement in terms of regeneration rate. The mass transfer coefficient of the different solutions has similar values when operating under the same conditions.
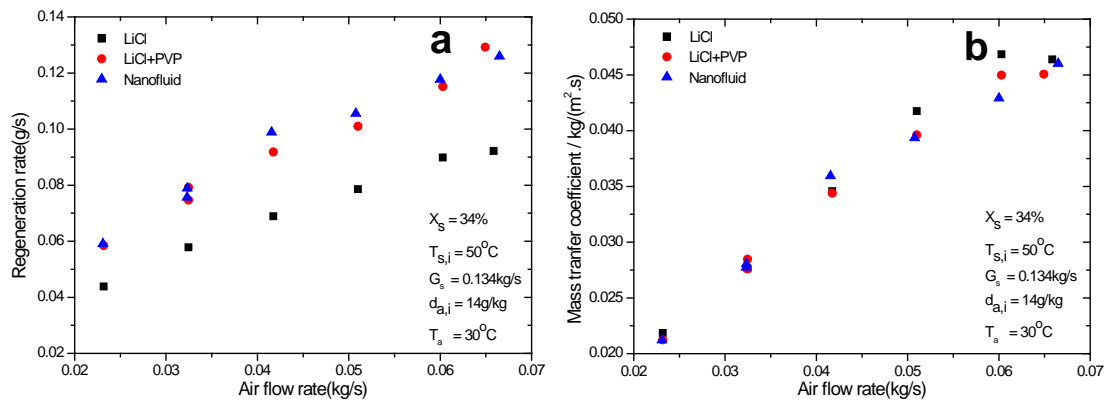

Fig. 9. Influence of air flow rate on regeneration performance.

3.5 Influence of air humidity

By analysing the experimental points in Fig. 10, we can see that the regeneration rate clearly decreases when the air humidity increases. When the air humidity increases, the mass transfer driving force (the difference between the air humidity and equivalent water vapour content at the surface of the solution) has a corresponding decrease. Consequently, the regeneration rates show a decreasing trend, as indicated in Fig. 10. Different degrees of regeneration improvement are also presented in this figure for solutions containing surfactant and nanoparticles, which is consistent with the results in Figs. 6 to 9, and for the influence of nanoparticles alone. The mass transfer coefficient also decreases gradually with air humidity, as shown in Fig. 10-b. The LiCl/H$_2$O-PVP solution and nanofluid have comparable mass transfer coefficients, which are slightly greater than that of the LiCl solution.
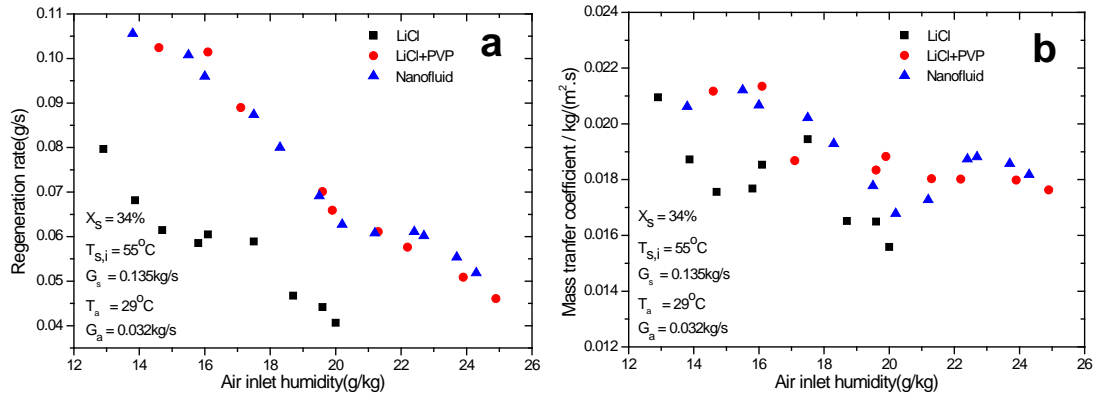
Fig. 10. Influence of air humidity on regeneration performance.

3.6 Discussion

It is clear that the LiCl/H_2O-PVP solution and nanofluid can enhance the regeneration rate compared with the ordinary LiCl/H_2O solution, as is adequately demonstrated by the experimental data in Figs. 6 to 10. The average relative improvements are 24.9% and 24.7% for LiCl/H_2O-PVP solution and nanofluid, respectively, under the same operating conditions. According to measurements of falling film characteristics, the improvement can be attributed to an increase in the wetting area and decrease of falling film thickness, as also mentioned in our research on dehumidification [31]. The wettability of different solutions on the plate regenerator was measured by a high resolution infrared thermal imager made by the FLUKE company. The wetting area increases from 0.172m^2 for the LiCl/H_2O solution to 0.209 m^2 for the LiCl/H_2O-PVP solution (a relative increase of 21.5%) and 0.210 m^2 for nanofluid (a relative increase of 22.1%). A greater wetting area can directly contribute to a higher regeneration rate, due to the greater contact area between the solution and air. The film thickness was obtained by a JDC-2008 accumeasure instrument with an accuracy of 0.8μm. Fig. 11 shows the variation of the film thickness with the change of time. A reduction of nearly 0.1 mm for both the two modified solutions from 0.681 mm to 0.583 mm and 0.577 mm is illustrated in Fig. 11. The decrease of film thickness can result in increased heat transfer efficiency between the solution and hot water, and an increased regeneration rate. In fact, both of these two contributors are closely related to the reduction of the contact angle, which was measured by a standard contact angle goniometer with a 0.1° resolution. The contact angle results are shown in Table 4. More than 30° reductions are observed for both the LiCl/H_2O-PVP solution and nanofluid. The decrease in contact angle can directly increase the wetting area and subsequently lead to a reduction in film thickness.

Comparing the regeneration rate between the LiCl/H_2O-PVP solution and nanofluid shows no obvious mass transfer enhancement in MWNTs. Even though the nanofluid regeneration rate increased up to 24.7% compared with the LiCl/H_2O solution, the enhancement resulted from adding 0.4 wt% surfactant for the purpose of dispersion stability in the nanofluid. This conclusion may seem inconsistent with the findings discussed in the earlier literature review. In the authors' limited understanding, there are two possible explanations for this discrepancy. First, many studies study the heat and mass transfer performance of nanofluid. However, most have failed to investigate the effect of surfactant alone and compare it with that of nanofluid. Second, the present study's experiments concerning liquid desiccant regeneration were carried out under an atmospheric pressure very different from that for absorption refrigerant. Absorption referigerant operates under much lower absolute pressure with a high vacuum degree. Moreover, our previous study also revealed the negligible influence of 0.4% MWNTs on thermal conductivity [35]. These factors together lead to a negligible effect of nanofluid on regeneration performance in the present study.

Moreover, as Figures 6 to 10 show, all three solutions have nearly the same mass transfer coefficient in comparable experimental conditions. This result is consistent with the conclusion that the enlargement of the wetting area is the main contributor to mass transfer enhancement. As the definition of the mass transfer coefficient in Equation (3) shows, the regeneration rate is exactly the numerator of the mass transfer coefficient. By adopting a surfactant, the wetting areas of the LiCl/H_2O-PVP solution and nanofluid increase significantly, and so does the regeneration rate. The wetting area is part of the denominator in the mass transfer coefficient. The comprehensive interaction of the regenerator in the numerator and wetting area in the denominator leads to a comparable mass transfer coefficient for different solutions.
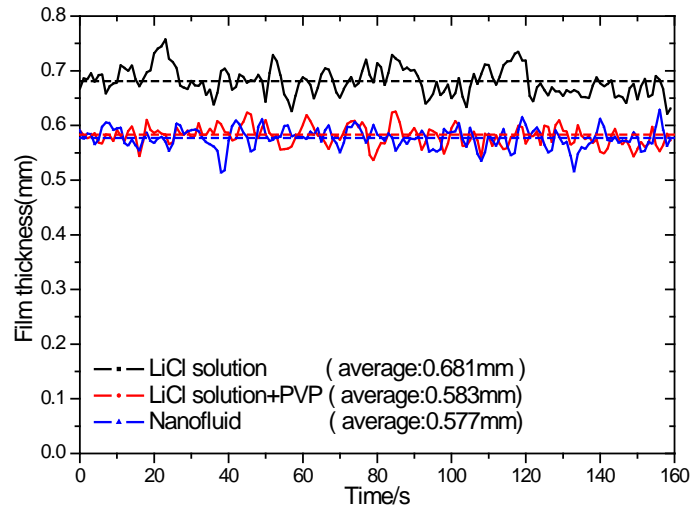
Fig. 11. Film thickness of different solutions on plate regenerator.

Table 4. Contact angles of different solutions.

Solution	Contact angle (°)
LiCl	58.5
LiCl + PVP	28.0
Nanofluid	26.5

4 Mathematical models development

4.1 Film shrinkage model

We included wettability in the earlier description because the falling film shrinks along the flow direction in the plate regenerator. Nevertheless, few studies related to plate type regeneration have taken the film contraction into consideration when building a mathematical model. Combined with our research group's previous studies [36, 37], the shrinkage model for the three kinds of solutions is established in this section.

The flow characteristics of falling film on plate are illustrated in Fig. 12. According to Levich [38], the governing equations and boundary conditions for falling film on plate are as follows:

$$\begin{cases} \dfrac{\partial p}{\partial y} = \mu \dfrac{\partial^2 u_y}{\partial^2 z} \\ \int_0^\delta u_y dz = 0 \end{cases} \tag{7}$$

$$\begin{cases} z = 0, \quad u_y = 0; \\ z = \delta, \quad \mu \dfrac{\partial u_y}{\partial z} = grad\sigma \end{cases} \tag{8}$$
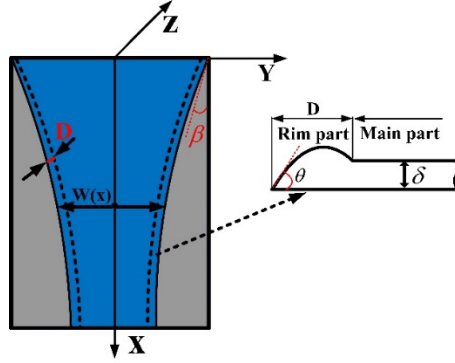

Fig. 12. Schematic diagram of falling film on plate.

Equation (9) is based on a vital hypothesis on the surface tension gradient ($grad\sigma$) from Zhang et al. [39], that the surface tension parallels the plate and decreases linearly from the rim to the central part over the length D.

$$grad\sigma = \frac{\sigma_m - \sigma_r \cos\theta}{D} \cos\beta \tag{9}$$

The angle β and rim length D are calculated by Equations (10) and (11), respectively.

$$\cos\beta = \frac{u_x}{\sqrt{u_x^2 + u_y^2}} \tag{10}$$

$$D = \frac{\xi\delta \sin\theta}{1 - \cos\theta} + \delta\sqrt{\frac{2\xi}{1 - \cos\theta}(\xi - 1) - (\xi - 1)^2} \tag{11}$$

Using the Nusselt Equation [40], the film thickness δ and velocity u_x can be formulated as follows:

$$\delta = \left(\frac{3G_s\mu_s}{W(x)\rho_s^2 g}\right)^{1/3} \tag{12}$$

$$u_x = \frac{1}{2}\frac{\rho_s g}{\mu_s}\delta^2 \tag{13}$$

Combining Equations (7) to (13), the width of falling film at x position can be calculated using Equation (14).

$$W(x) = W - \sqrt{2} \int_0^{x_0} \sqrt{\sqrt{1 + \frac{4(\frac{\delta}{4\mu_s D}(\sigma_m - \sigma_r \cos\theta))^2}{u_x^2}} - 1} \ dx \qquad (14)$$

The thermal properties of the LiCl/H$_2$O solution are obtained from equations provided by Conde [33]. For a 0.4 wt% LiCl/H$_2$O-PVP solution, the PVP density is 1.144 g/cm^3, which is very close to the density of 1.206 g/cm^3 for the 34 wt% LiCl/H$_2$O solution adopted in the present study. Given its small content level, the density of the LiCl/H$_2$O-PVP solution and nanofluid was considered the same as that of the LiCl/H$_2$O solution. Two other physical properties of the LiCl/H$_2$O-PVP solution, namely dynamic viscosity and surface tension, were obtained by multiplying the original values of the LiCl/H$_2$O solution by certain factors. To determine these factors, the dynamic viscosity and surface tension were measured for the LiCl/H$_2$O-PVP solution and nanofluid. A rotational viscometer and a surface tension meter based on the pendant-drop method were used to measure the properties. The results are shown in Table 5. The factor is the quotient of the value for the modified solution and the original one. The calculated factors for dynamic viscosity and surface tension are 1.095 and 0.746 for the LiCl/H$_2$O-PVP solution, and 1.107 and 0.723 for nanofluid.

Table 5. Physical properties of solutions

Solution	Dynamic viscosity (mPa.s)	Surface tension (*10^{-3}N/m)
LiCl	4.20	93.51
LiCl + PVP	4.60	69.84
Nanofluid	4.65	67.61

4.2 Regeneration model

Several commonly adopted assumptions are made in the present model for regeneration, as follows:

(1) The film thickness is consistent in one microelement, and perpendicular to the falling film flow direction.

(2) The physical properties are consistent in one microelement.

(3) The wall temperature is the same as the heating water temperature because of the high thermal conductivity of the material and thin wall thickness.

(4) The regenerator is insulated from the ambient environment.

According to these assumptions, the mass balance equations for air and solution can be formulated as:

$$G_a dw_a - \alpha_m (w_a - w_e) W(x) dx = 0 \tag{15}$$

$$dG_s - G_a dw_a = 0 \tag{16}$$

The energy conservation equations for air, solution and heating water are severally described by Equations (17), (18) and (19).

$$G_a c_{p,a} dT_a - \alpha_{h,a} (T_a - T_s) W(x) dx = 0 \tag{17}$$

$$G_a dh_a + d(G_s h_s) + G_w c_{p,w} dT_w = 0 \tag{18}$$

$$G_w c_{p,w} dT_w - \alpha_{h,w} (T_w - T_s) W(x) dx = 0 \tag{19}$$

The enthalpy change of air in Equation (18) is given by Equation (20):

$$dh_a = c_{p,a} dT_a + ((c_{p,a} + (c_{p,v} - c_{p,a}) w_a) T_a + w_a \gamma)) dw_a \tag{20}$$

By adopting the empirical correlations (21) and (22), the heat transfer coefficient α_h [41] and mass transfer coefficient α_m [42] can be calculated.

$$\alpha_h = 0.664 * Re^{1/2} Pr^{1/3} \tag{21}$$

$$\alpha_m = 0.0139 * Re_a^{0.75} * Sc_a^{4.81} * d_{a,i}^{-0.53} d_e^{-0.68} * \rho_a * D / d_e \quad LiCl / H_2O \ solution$$

$$\alpha_m = 0.0146 * Re_a^{0.75} * Sc_a^{4.81} * d_{a,i}^{-0.53} d_e^{-0.68} * \rho_a * D / d_e \quad LiCl / H_2O\text{-}PVP \ solution \ and \ nanofluid \tag{22}$$

4.3 Model validation

By integrating Equations (10) to (22), the flow characteristics and heat and mass transfer performance of the falling film regenerator can be solved numerically. To validate the constructed models, wettability and regeneration rate tests were carried out individually. Two criteria, Mean Relative Deviation (MRD) and Mean Absolute Relative Deviation (MARD), are used to evaluate the deviations between calculated regeneration rate Δm_{cal} and experimental regeneration rate Δm_{exp}.

$$MRD = \frac{1}{N} \sum_{i=1}^{N} \frac{\Delta m_{cal} - \Delta m_{exp}}{\Delta m_{exp}} \tag{23}$$

$$MARD = \frac{1}{N}\sum_{i=1}^{N}\left|\frac{\Delta m_{cal} - \Delta m_{exp}}{\Delta m_{exp}}\right| \qquad (24)$$

The contrast between the infrared images and the computational flow shapes are illustrated in Fig. 13. Table 6 details the measured wetting areas and calculated areas and their derivations. As one can see, the models give accurate predictions for both the shrinkage shape and wetting area, with a maximum absolute relative deviation of less than 6%.
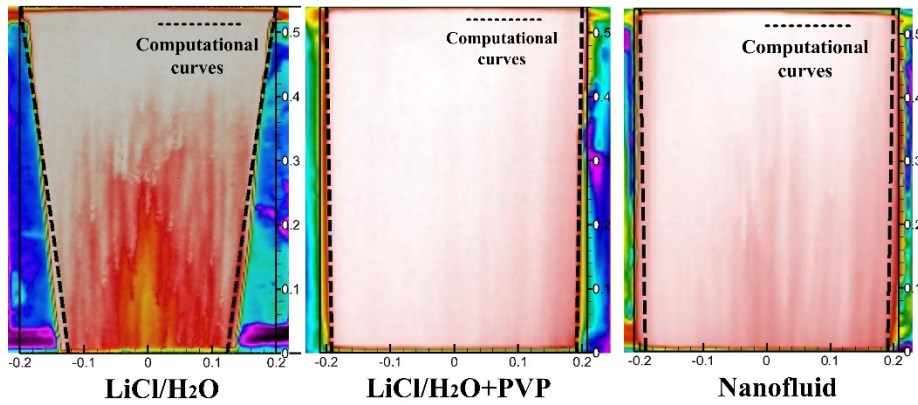

Fig. 13. Measured and computational wettability of different solutions.

Table 6. Comparison between the measured and calculated wetting areas.

Solution	Measured wetting area (m^2)	Calculated wetting area (m^2)	Relative derivation
LiCl	0.172	0.162	-5.81%
LiCl + PVP	0.209	0.210	0.55%
Nanofluid	0.210	0.212	0.95%

The regeneration rate for these three kinds of solutions were also checked. Fig. 14 compares the experimental and calculated values. Almost all of the MRDs fall into the error band of $\pm 15\%$ for the three solutions. Even the greatest MARD, for the LiCl/H$_2$O solution, is less than 10%, which is mainly caused by somewhat poor prediction accuracy for the wetting area. For both the LiCl/H$_2$O-PVP solution and nanofluid, the MARD is less than 5%. Consequently, not only the wettability but also the mass transfer performance of the falling film regenerator can be accurately predicted by the model proposed in this study.
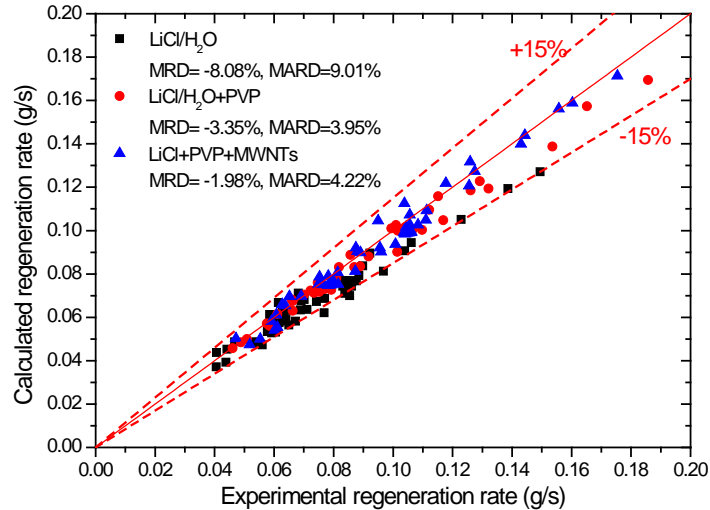
Fig. 14. Comparison between the experimental and calculated regeneration rate.

5 Conclusion

The present study experimentally identified the regeneration performance of LiCl/H_2O solution, LiCl/H_2O-PVP solution and LiCl/H_2O-MWNTs nanofluid under various working conditions. A mathematical model that takes film contraction into consideration was also newly established and validated. Based on experimental results and numerical simulations, conclusions were drawn as follows:

(1) The average relative regeneration rate enhancements are 24.9% and 24.7% for LiCl/H_2O-PVP solution and nanofluid, respectively, compared with LiCl/H_2O solution under the same operating conditions. However, the effect on the regeneration rate of adding 0.1 wt% MWNTs is negligible. Therefore, adding PVP into liquid desiccant can be an effective way of enhancing the regeneration rate. However, the mass transfer coefficients for the three solutions are almost the same under comparable experimental conditions.

(2) The regeneration rate improvement can be attributed to the addition of surfactant PVP. Adding PVP reduces the contact angles for the two modified solutions by approximately 30° from the original 58.5°. Consequently, the wetting area increases and falling film thickness decreases, which benefits the mass transfer process.

(3) The developed model, which takes film shrinkage on the plate regenerator into

consideration, can accurately simulate both the wettability and regeneration rate. The greatest MARDs for the wetting area and regeneration rate among these three solutions are 5.81% and 9.01% for the LiCl/H$_2$O solution. For the other two modified solutions, the prediction deviations are less than 1% for the wetting area and 5% for the regeneration rate.

The comparative experimental results for the three different solutions in this study are valuable for studying mass transfer enhancement by adding surfactant and nanoparticles. The mathematical models developed provide a practical and accurate method for the study and design of plate type regenerators and LDCS.

Acknowledgement

References

[1] Abdel-Salam A.H., Simonson C.J., State-of-the-art in liquid desiccant air conditioning equipment and systems, Renewable and Sustainable Energy Reviews, 58 (2016) 1152-1183.

[2] Yin Y., Qian J., Zhang X., Recent advancements in liquid desiccant dehumidification technology, Renewable and Sustainable Energy Reviews, 31 (2014) 38-52.

[3] Wan K.K., Li D.H., Liu D., Lam J.C., Future trends of building heating and cooling loads and energy consumption in different climates, Building and Environment, 46 (2011) 223-234.

[4] Isshiki N., Ogawa K., Enhancement of heat and mass transfer by CCS tubes, Ab-Sorption 96, Proceedings of the ISHPC, Montreal, Canada.[Links], (1996).

[5] Park C.W., Kim S.S., Cho H.C., Kang Y.T., Experimental correlation of falling film absorption heat transfer on micro-scale hatched tubes, International journal of refrigeration, 26 (2003) 758-763.

[6] Yoon J.-I., Kwon O.-K., Moon C.-G., Experimental investigation of heat and mass transfer in absorber with enhanced tubes, KSME International Journal, 13 (1999) 640-646.

[7] Cui X.-Y., Shi J.-Z., Tan C., Xu Z.-P., Investigation of plate falling film absorber with film-inverting configuration, Journal of Heat Transfer, 131 (2009) 072001.

[8] Islam M.R., Wijeysundera N., Ho J., Performance study of a falling-film absorber with a film-inverting configuration, International Journal of Refrigeration, 26 (2003) 909-917.

[9] Mortazavi M., Isfahani R.N., Bigham S., Moghaddam S., Absorption characteristics of falling film LiBr (lithium bromide) solution over a finned structure, Energy, 87 (2015) 270-278.

[10] Dong C., Lu L., Wen T., Experimental study on dehumidification performance enhancement by TiO2 superhydrophilic coating for liquid desiccant plate dehumidifiers, Building and Environment, 124

(2017) 219-231.

[11] Hihara E., Saito T., Effect of surfactant on falling film absorption, International journal of refrigeration, 16 (1993) 339-346.

[12] Glebov D., Setterwall F., Experimental study of heat transfer additive influence on the absorption chiller performance, International journal of refrigeration, 25 (2002) 538-545.

[13] Kang Y.T., Kashiwagi T., Heat transfer enhancement by Marangoni convection in the NH 3–H 2 O absorption process, International Journal of Refrigeration, 25 (2002) 780-788.

[14] Kashiwagi T., Basic mechanism of absorption heat and mass transfer enhancement by the Marangoni effect, Newsletter, IEA Heat Pump Center, 6 (1988) 2-6.

[15] Daiguji H., Hihara E., Saito T., Mechanism of absorption enhancement by surfactant, International journal of heat and mass transfer, 40 (1997) 1743-1752.

[16] Kang Y., Akisawa A., Kashiwagi T., Experimental investigation of Marangoni convection in aqueous LiBr solution with additives, Journal of heat transfer, 121 (1999).

[17] Kulankara S., Herold K.E., Theory of heat/mass transfer additives in absorption chillers, HVAC&R Research, 6 (2000) 369-380.

[18] Chol S., Enhancing thermal conductivity of fluids with nanoparticles, ASME-Publications-Fed, 231 (1995) 99-106.

[19] Yu W., France D.M., Routbort J.L., Choi S.U., Review and comparison of nanofluid thermal conductivity and heat transfer enhancements, Heat Transfer Engineering, 29 (2008) 432-460.

[20] Sergis A., Hardalupas Y., Anomalous heat transfer modes of nanofluids: a review based on statistical analysis, Nanoscale research letters, 6 (2011) 391.

[21] Godson L., Raja B., Lal D.M., Wongwises S., Enhancement of heat transfer using nanofluids—an overview, Renewable and sustainable energy reviews, 14 (2010) 629-641.

[22] Pang C., Lee J.W., Kang Y.T., Review on combined heat and mass transfer characteristics in nanofluids, International Journal of Thermal Sciences, 87 (2015) 49-67.

[23] Kang Y.T., Kim H.J., Lee K.I., Heat and mass transfer enhancement of binary nanofluids for H 2 O/LiBr falling film absorption process, International Journal of Refrigeration, 31 (2008) 850-856.

[24] Kim H., Jeong J., Kang Y.T., Heat and mass transfer enhancement for falling film absorption process by SiO 2 binary nanofluids, International Journal of Refrigeration, 35 (2012) 645-651.

[25] Zhang L., Liu Y., Wang Y., Li H., Yang X., Jin L., Experimental Study on Enhanced Falling Film Absorption Process Using H2O/LiBr Nanofluids, in: ASME 2016 5th International Conference on Micro/Nanoscale Heat and Mass Transfer, American Society of Mechanical Engineers, 2016, pp. V001T002A012-V001T002A012.

[26] Yang L., Du K., Niu X.F., Cheng B., Jiang Y.F., Experimental study on enhancement of ammonia–water falling film absorption by adding nano-particles, International journal of refrigeration, 34 (2011) 640-647.

[27] Pineda I.T., Lee J.W., Jung I., Kang Y.T., CO 2 absorption enhancement by methanol-based Al 2 O 3 and SiO 2 nanofluids in a tray column absorber, International journal of refrigeration, 35 (2012) 1402-1409.

[28] Ali A., Vafai K., Khaled A.-R., Analysis of heat and mass transfer between air and falling film in a cross flow configuration, International Journal of Heat and Mass Transfer, 47 (2004) 743-755.

[29] Ali A., Vafai K., An investigation of heat and mass transfer between air and desiccant film in an inclined parallel and counter flow channels, International Journal of Heat and Mass Transfer, 47 (2004) 1745-1760.

[30] Bouguerra N., Poncet S., Elkoun S., Dispersion regimes in alumina/water-based nanofluids: Simultaneous measurements of thermal conductivity and dynamic viscosity, International Communications in Heat and Mass Transfer, 92 (2018) 51-55.

[31] Tao Wen L.L., Hong Zhong, Investigation on the dehumidification performance of LiCl/H2O-MWNTs nanofluid in liquid desiccant cooling system, Energy and Buildings(Submitted).

[32] Wen T., Lu L., Dong C., Luo Y., Development and experimental study of a novel plate dehumidifier made of anodized aluminum, Energy, 144 (2018) 169-177.

[33] Conde M.R., Properties of aqueous solutions of lithium and calcium chlorides: formulations for use in air conditioning equipment design, International Journal of Thermal Sciences, 43 (2004) 367-382.

[34] Coleman H.W., Steele W.G., Experimentation, validation, and uncertainty analysis for engineers, John Wiley & Sons, 2009.

[35] Wen T., Lu L., Zhong H., Investigation on the dehumidification performance of LiCl/H 2 O-MWNTs nanofluid in a falling film dehumidifier, Building and Environment, (2018).

[36] Dong C., Lu L., Qi R., Model development of heat/mass transfer for internally cooled dehumidifier concerning liquid film shrinkage shape and contact angles, Building and Environment, 114 (2017) 11-22.

[37] Qi R., Lu L., Yang H., Qin F., Influence of plate surface temperature on the wetted area and system performance for falling film liquid desiccant regeneration system, International Journal of Heat and Mass Transfer, 64 (2013) 1003-1013.

[38] Levich V.G., Physicochemical hydrodynamics, Prentice hall, 1962.

[39] Zhang F., Zhang Z., Geng J., Study on shrinkage characteristics of heated falling liquid films, AIChE journal, 51 (2005) 2899-2907.

[40] Nusselt W., Dia Oberflachen condensation des wasserdampfes, Zeitchrift des Vereines deustcher Ingenieure, 60 (1916) 1645-1648.

[41] Patankar S., Numerical heat transfer and fluid flow, CRC press, 1980.

[42] Tao Wen L.L., Chuanshuai Dong, Yimo Luo, Investigation on the regeneration performance of liquid desiccant by adding surfactant PVP-K30, International Journal of Heat and Mass Transfer, 123 (2018) 445-454.